17

Deforming: Plasticity

CHAPTER PREVIEW

In this chapter we are concerned with the deformation of ceramics leading to a permanent shape change. This is known as plastic deformation and is both nonrecoverable and irreversible. There are several mechanisms that are responsible for plastic deformation in crystalline materials: dislocation motion, vacancy motion, twinning, and phase transformation. In metals at room temperature dislocation motion is the most important of these mechanisms. In Chapter 12 we already noted that dislocations do not move easily in ceramics and this is the reason for their inherent brittleness. Nevertheless, dislocation motion is observed in ceramics under specific loading conditions. In general, plastic deformation of ceramics requires high temperatures and this is important because

- We often process ceramics at high temperature.
- Many potential applications for ceramics, such as in fuel cells and engines, require them to be stable at high temperature.

We know that glass flows and that we can produce complex shape changes in glass. There are no dislocations in glass so how does plastic deformation occur? And does the plastic deformation of glass always require a high temperature?

Selecting ceramics for use at high temperatures or under applied load requires consideration of their long-term stability. Time dependent deformation is known as creep, and creep resistance is a critical design parameter. Even if creep does not lead to failure, a change in shape or size may render a component useless. The mechanism responsible for creep depends on temperature, stress, and the microstructure of the ceramic.

17.1 PLASTIC DEFORMATION

The onset and extent of plastic deformation are often measured when the σ–ε behavior of a material is being determined. We showed some general σ–ε curves in Chapter 16. In Figure 17.1 σ–ε curves obtained for crystals of KBr and MgO tested in bending are shown. From these curves we can identify several parameters that may already be familiar to you from the discussion of the mechanical properties of metals.

The proportional limit P corresponds to departure from linearity and is defined as the onset of plastic deformation. If the transition from elastic to plastic deformation is gradual it may be difficult to determine precisely where P is and sometimes it is better avoided.

The yield strength σ_y is the stress determined by drawing a line parallel to the linear part of the σ–ε curve at some specified strain offset. We usually use a strain of 0.002. To compare the values of σ_y in Figure 17.1 you may recall that for metals we see a wide range of values, e.g., for a low-strength aluminum alloy $\sigma_y = 35\,\text{MPa}$ and for a high-strength steel $\sigma_y > 1400\,\text{MPa}$. We usually say yield strength rather than yield stress. Strength is a material property; stress is a measure of the applied load.

Fracture strength, σ_F, is the stress at a fracture. Because ceramics are often tested in bending we do not see any reduction in cross-sectional area during the test as we often see in a tensile test with a metal. As a result we would not expect to see a maximum in the σ–ε curve corresponding to the tensile strength or ultimate tensile strength.

Figure 17.2 shows a σ–ε curve for LiF that illustrates an abrupt elastic–plastic transition. Plastic deformation begins at the upper yield point and there is a decrease in stress. At the lower yield point deformation continues at lower stress levels. This type of behavior is similar to that of some low-carbon steels as well as aluminum oxide and magnesium oxide at high temperatures.

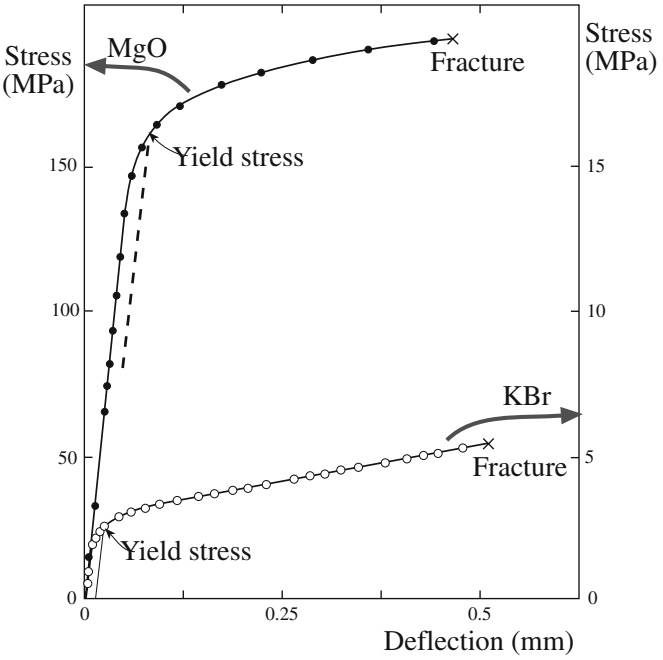

FIGURE 17.1 Stress–strain curves for KBr and MgO crystals tested in bending.

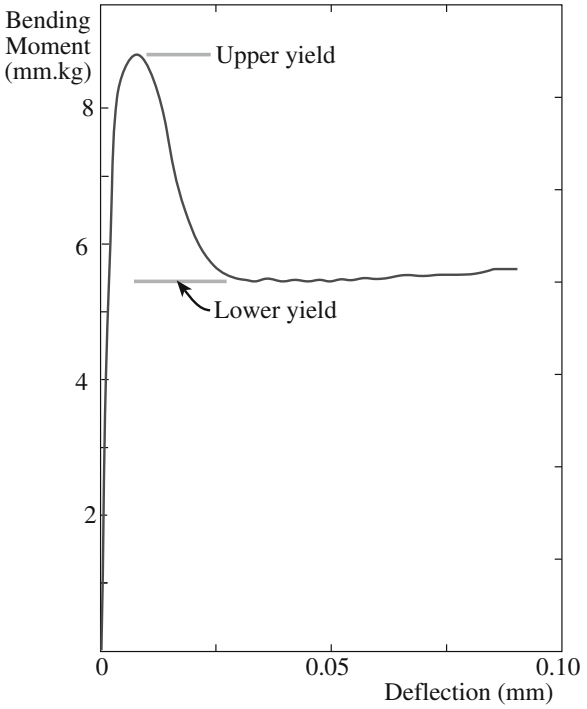

FIGURE 17.2 Stress–strain curve for a LiF single crystal.

17.2 DISLOCATION GLIDE

Dislocation glide (or slip) is a primary mechanism for plastic deformation in crystals. Slip takes place discontinuously in bands as illustrated in Figure 17.3. Although we often think of dislocations in ceramics as immobile, they can glide as shown in Figure 17.4a. In this case a crystal of LiF has been plastically bent and the dislocations revealed by etching. Figure 17.4b is a dark-field transmission electron microscopic (TEM) image that shows a glide band in spinel. The dislocations are visible in the dark-field image as bright lines against a dark background.

Both the direction of slip and usually the slip plane have a definite crystallographic orientation, which together are known as a slip system. Slip systems for several ceramics are given in Table 17.1. Primary slip systems are those for which slip is easiest; it is more difficult on secondary slip systems and these are usually activated at higher temperature. What determines the slip system for ceramics?

SLIP SYSTEM

A slip system is a plane and a direction and is represented as {*hkl*}<*uvw*>.

The slip direction is usually the direction having the smallest spacing between atoms or ions of the same type (the highest linear density). In metals, the slip plane is often the closest packed plane (the highest planar density). In ceramics, we consider planar density, but there is often the additional consideration of electrostatic interaction between ions. We can illustrate these considerations by looking at the familiar rocksalt structure (structure of NaCl and MgO). This is an interesting example to choose to start with because the first studies of crystal plasticity, which were conducted by Reusch in 1867, were conducted using sodium chloride. He concluded that the slip system for NaCl is {110}<1$\bar{1}$0>.

The choice of slip plane has often been explained by considering the position of ions during slip. Figure 17.5 compares the ion positions during slip on {100} and {110}. The key difference is that slip on {100} would increase the distance between opposite ions. However, during slip on {110} oppositely charged ions are brought closer together. The overall effect is that slip on {110} would lead to a decrease in the electrostatic interaction energy. Clearly this is not the complete story as we mentioned in Section 12.5. Not all crystals with a rocksalt structure share the same slip system as shown in Table 17.2. The primary glide plane depends on the atoms present. For PbS and PbTe the primary glide plane is {100} not {110}. The explanation proposed back in 1930 by Buerger is based on the polarizability or "deformability" of the ions. As the sum of the polarizability of both ions increases there is increasing ease of slip on {100} and increasing plasticity.

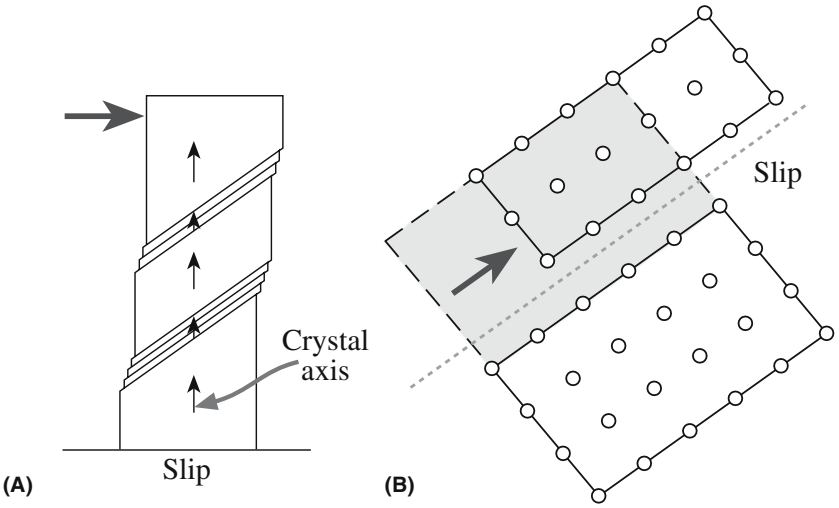

FIGURE 17.3 Illustration of slip bands: (a) macroscopic appearance; (b) showing atomic movements.

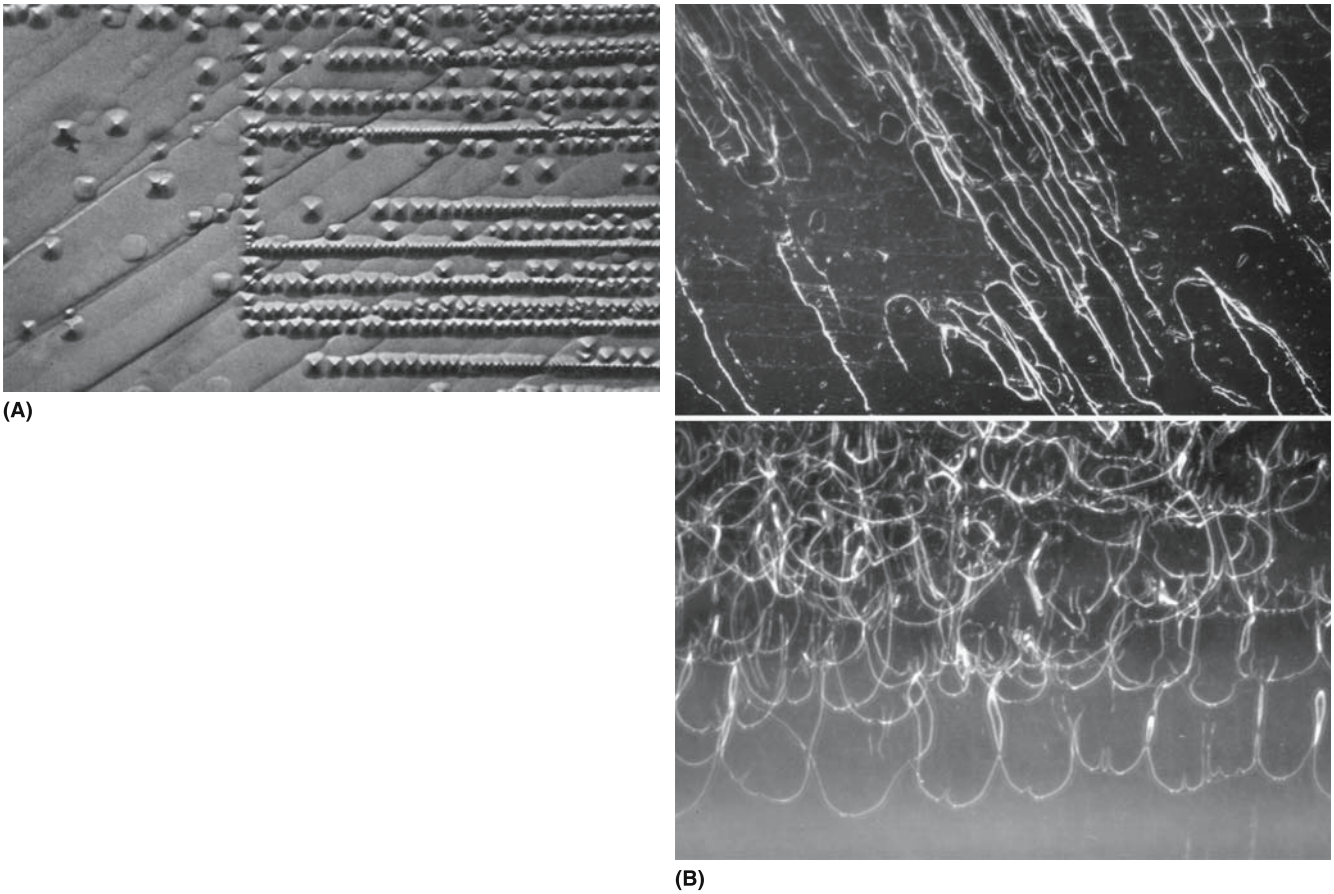

FIGURE 17.4 (a) Glide bands in LiF revealed by etching. (b) "Glide" bands in spinel: (top) 200°C; (bottom) 950°C.

TABLE 17.1 Slip Systems for Several Ceramics

Material	Crystal structure	Slip systems		Activation temperature (°C)	
		Primary	Secondary	Primary	Secondary
Al_2O_3	Hexagonal	{0001}<11$\bar{2}$0>	Several	1200	
BeO	Hexagonal	{0001}<11$\bar{2}$0>	Several	1000	
MgO	Cubic (NaCl)	{110}<1$\bar{1}$0>	{001}<110>	0	1700
$MgO \cdot Al_2O_3$	Cubic (spinel)	{111}<1$\bar{1}$0>	{110}<1$\bar{1}$0>	1650	
β-SiC	Cubic (ZnS)	{111}<1$\bar{1}$0>		>2000	
β-Si_3N_4	Hexagonal	{10$\bar{1}$0}<0001>		>1800	
TiC, (ZrC, HfC, etc.)	Cubic (NaCl)	{111}<1$\bar{1}$0>	{110}<1$\bar{1}$0>	900	
UO_2, (ThO_2)	Cubic (CaF_2)	{001}<110>	{110}<1$\bar{1}$0>	700	1200
ZrB_2 (TiB_2)	Hexagonal	{0001}<11$\bar{2}$0>		2100	
C (diamond)	Cubic	{111}<1$\bar{1}$0>			
C (graphite)	Hexagonal	{0001}<11$\bar{2}$0>			
β-SiO_2	Hexagonal	{0001}<11$\bar{2}$0>			
CaF_2 (BaF_2, etc.)	Cubic	{001}<110>			
CsBr	Cubic (CsCl)	{110}<001>			
TiO_2	Tetragonal	{110}<1$\bar{1}$0>	{110}<001>		
WC	Hexagonal	{10$\bar{1}$0}<0001>	{10$\bar{1}$0}<11$\bar{2}$0>		

17.3 SLIP IN ALUMINA

The slip system for α-alumina (corundum) is given in Table 17.1. The primary slip plane is the basal plane, (0001); the slip direction is <11$\bar{2}$0>. The arrangement of atoms on the slip plane was shown in Figure 12.12. For the oxygen ions the close-packed direction is actually <1$\bar{1}$00>; this is not the slip direction because we need to consider what happens to the aluminum ions, which occupy only two-thirds of the octahedral interstices. Slip along <11$\bar{2}$0> preserves the stacking sequence of the aluminum ions. Temperatures around 1300°C are needed before significant plastic deformation is observed in single-crystal alumina. At even higher temperatures other slip systems become activated as summarized in Table 17.3.

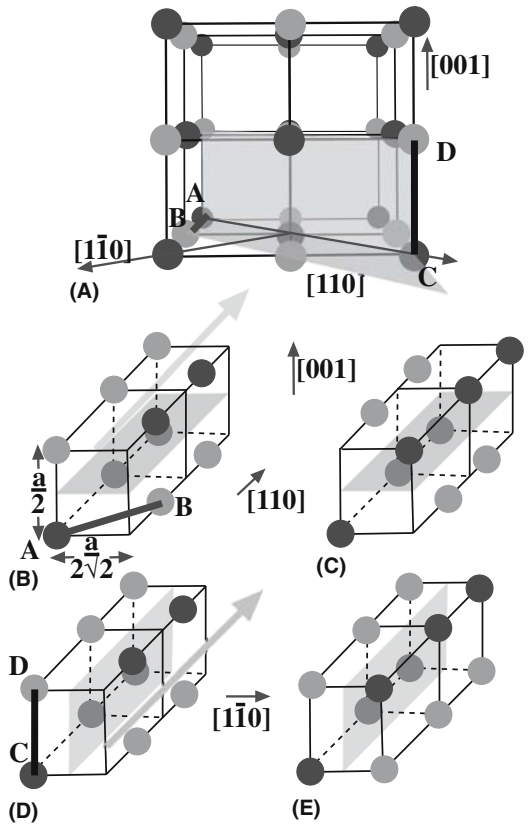

FIGURE 17.5 (a–e) Schematic comparing slip in the rocksalt structure on {100} and {110} planes.

TABLE 17.2 Comparison of Primary Glide Planes in Crystals Having a Rocksalt Structure

Crystal	Primary glide plane	Polarizability ($10^{-30}/m^3$)			Lattice constant (nm)
		Anion	Cation	Total	
LiF	{110}	0.03	1.0	1.03	0.401
MgO	{110}	0.09	3.1	3.19	0.420
NaCl	{110}	0.18	3.7	3.88	0.563
PbS	{100}	3.1	10.2	13.3	0.597
PbTe	{100}	3.1	14.0	17.1	0.634

TABLE 17.3 Slip Systems in α-Alumina (Corundum)

System name	Slip system	Remarks
Basal	(0001)1/3<2$\bar{1}\bar{1}$0>	Dominant system under shear superimposed on 1-atm pressure
Prismatic	{1$\bar{2}$10}<10$\bar{1}$0> {1$\bar{2}$10}<10$\bar{1}$1>	Occurs above 1600°C under shear superimposed on 1-atm pressure
Pyramidal	{1$\bar{1}$02}<01$\bar{1}$1> {10$\bar{1}$1}<01$\bar{1}$1>	Occurs above 1600°C under shear superimposed on 1-atm pressure

Because of the large Burgers vector involved the combined motion of partial dislocations may lead to slip. The background to this argument was presented in Chapter 12. Graphite is another hexagonal ceramic in which slip has been found to occur by the motion of partial dislocations.

17.4 PLASTIC DEFORMATION IN SINGLE CRYSTALS

There are many mechanisms that can lead to plastic deformation in single crystals, but the most important is slip. The two things that we need to consider are the inherent resistance to the movement of dislocations provided by the periodicity of the lattice and the orientation of the crystal with respect to the applied stress.

Lattice Resistance

The stress, τ_f, needed to move a dislocation along the slip plane is known as the Peierls–Nabarro (or frictional) stress and is given by

$$\tau_f = \mu \exp\left(-\frac{2\pi w}{b}\right) \tag{17.1}$$

The stress, which is clearly a function of the crystal structure and bonding, depends on b and w. You will recall from Chapter 12 that dislocation widths in covalent solids are quite narrow ($w \sim b$) compared with those in face-centered cubic (fcc) metals ($w \sim 10b$).

- For metals $\tau_f \sim 10\,\text{MPa} \sim 10^{-4}\mu$, these stresses are fairly small and dislocations can move freely. The yield stress is determined primarily by interactions between dislocations and other defects such as impurities.
- For simple ionic ceramics (e.g., NaCl and CaF_2) $\tau_f \sim 10\text{–}100\,\text{MPa} \sim 10^{-4}\mu\text{–}10^{-3}\mu$.
- For complex ionic (e.g., Al_2O_3) and covalent ceramics (e.g., SiC) $\tau_f \sim 1000\,\text{MPa} \sim 10^{-2}\mu$. Dislocations have low mobility and lattice resistance is the main obstacle.

Orientation

Plastic deformation depends not only on how easy it is for the dislocations to glide on their slip plane but also the orientation of the slip plane and the slip direction with the applied stress. If we consider a single crystal subject to uniaxial tension as illustrated in Figure 17.6 the shear stress, τ_r, acting on the slip plane in the slip direction is

$$\tau_r = \sigma \cos\phi \cos\psi \tag{17.2}$$

For some structures it is possible to orient the crystal so that τ_r on all operative slip systems is zero. If this is the case, dislocation motion does not occur and the crystal will not plastically deform at stresses below the theoretical lattice strength. For example, in MgO τ_r is zero when σ is applied along <111>. Under these loading conditions at elevated temperatures (>300°C) slip may occur on the secondary slip system: {001}<110>.

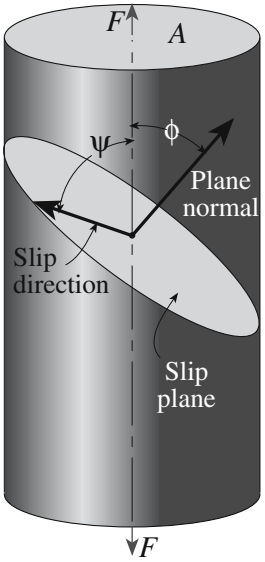

FIGURE 17.6 Geometry used to determine the critical resolved shear stress.

The critical resolved shear stress, τ_{crss}, is the minimum shear stress required to initiate slip for a particular slip system defined when $\sigma = \sigma_y$:

$$\tau_{crss} = \sigma_y(\cos\phi \cos\psi) \tag{17.3}$$

Figure 17.7a shows the stress–strain behavior for a single crystal that is favorably oriented for plastic flow. This type of behavior is seen in MgO and other ceramics with a rocksalt structure. There are three distinct stages:

- Stage I: Easy glide of dislocations with the possibility of large strains (~20%)
- Stage II: Interaction of dislocations on intersecting slip planes resulting in work hardening
- Stage III: Cross-slip

The value of τ_{crss} depends on test conditions such as temperature and strain rate as shown schematically in Figure 17.7b. We can again identify three distinct behaviors:

- Region I: τ_{crss} decreases with increasing temperature and decreasing strain rate. Thermal fluctuations enhance dislocation motion.

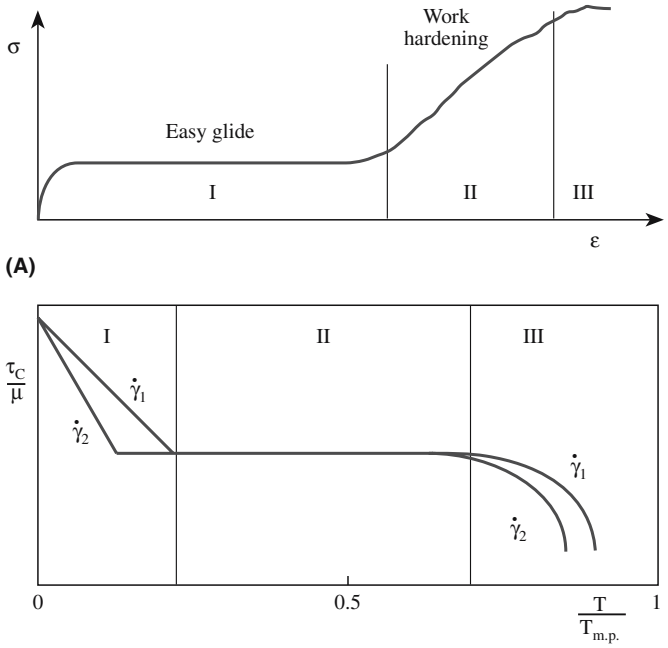

FIGURE 17.7 (a) Stress–strain curve for a crystal suitably oriented for plastic flow. (b) Temperature dependence of the normalized critical resolved shear stress for two strain rates, where $\gamma_1 > \gamma_2$.

- Region II: τ_{crss} is independent of temperature and strain rate. There is interaction between dislocations and between dislocations and other defects.
- Region III: τ_{crss} again decreases with increasing temperature and decreasing strain rate. At high temperatures diffusion processes can become important.

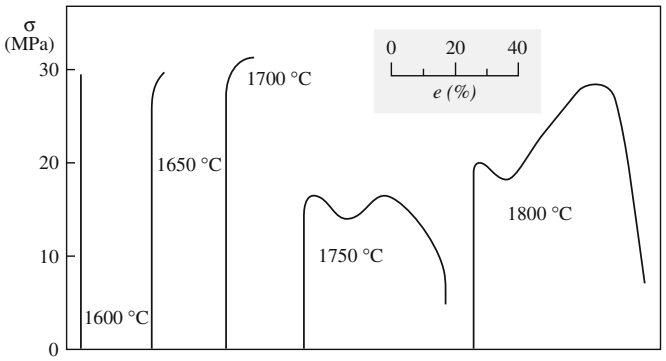

FIGURE 17.8 Stress–strain curves for polycrystalline MgO as a function of temperature.

17.5 PLASTIC DEFORMATION IN POLYCRYSTALS

Plastic deformation is more difficult in polycrystals than in single crystals because now we have to consider what happens at the grain boundaries. Grain boundaries act as barriers to dislocation motion and if adjacent grains are not favorably oriented for slip to continue, dislocations will pile up at the boundary.

A polycrystal needs five independent slip systems before it can undergo an arbitrary strain. This requirement is known as the von Mises criterion. A slip system is independent if the same strain cannot be produced from a combination of slip on other systems. From Table 17.4 you can see why MgO might be ductile when stressed as a single crystal but in polycrystalline form it is brittle except at high temperature where secondary slip systems operate. For polycrystalline MgO the brittle-to-ductile transition occurs at ~1700°C as shown in Figure 17.8.

TABLE 17.4 Independent Slip Systems for Some Ceramics

Lattice type	*Crystal*	*Slip system*	*Number of independent systems*
Rocksalt	MgO, NaCl, LiF, NaF	{110}<1$\bar{1}$0>	2
Rocksalt	MgO, NaCl, LiF, NaF	{110}<1$\bar{1}$0> {001}<1$\bar{1}$0> {111}<1$\bar{1}$0>	5 at high temperature
Fluorite	UO_2 and CaF_2	{001}<1$\bar{1}$0>	3
	TiC and UC	{111}<1$\bar{1}$0>	5
Spinel	$MgAl_2O_4$	{111}<1$\bar{1}$0> {110}<1$\bar{1}$0>	5
Fluorite	UO_2 and CaF_2	{001}<1$\bar{1}$0> {110}<1$\bar{1}$0> {111}<1$\bar{1}$0>	5 at high temperatures
Hexagonal	Al_2O_3, C (graphite), BeO	{0001}<11$\bar{2}$0>	2
Hexagonal	Al_2O_3, C (graphite), BeO	{0001}<11$\bar{2}$0> {1$\bar{2}$10}<10$\bar{1}$0> {1$\bar{2}$10}<10$\bar{1}$1> {1$\bar{1}$02}<01$\bar{1}$1> {10$\bar{1}$1}<01$\bar{1}$1>	5 at high temperatures
Sphalerite	ZnS, β-SiC	(111)<1$\bar{1}$0>	5

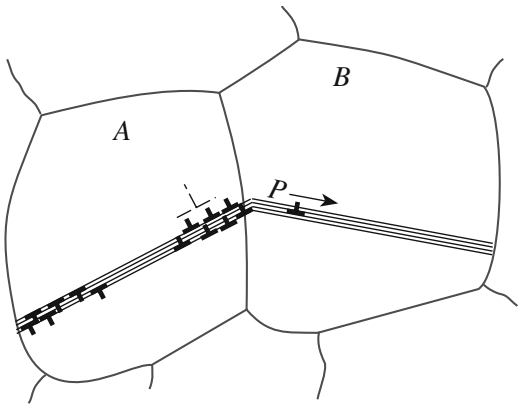

FIGURE 17.9 Illustration of slip propagation from grain A to grain B.

Some cubic materials, e.g., TiC and $MgAl_2O_4$, do have enough independent slip systems, but the Peierls–Nabarro stress is high making dislocations immobile except at high temperature.

The Hall–Petch relation (Eq. 14.8) indicates the effect of grain size, d, on the stress required to make the dislocation move in a polycrystalline sample. The origin of the relation is that the stress to operate a Frank–Read source increases as the size of the source decreases. If the grain size decreases, then the maximum size of the Frank–Read source also decreases. The result is the famous $d^{1/2}$ relationship.

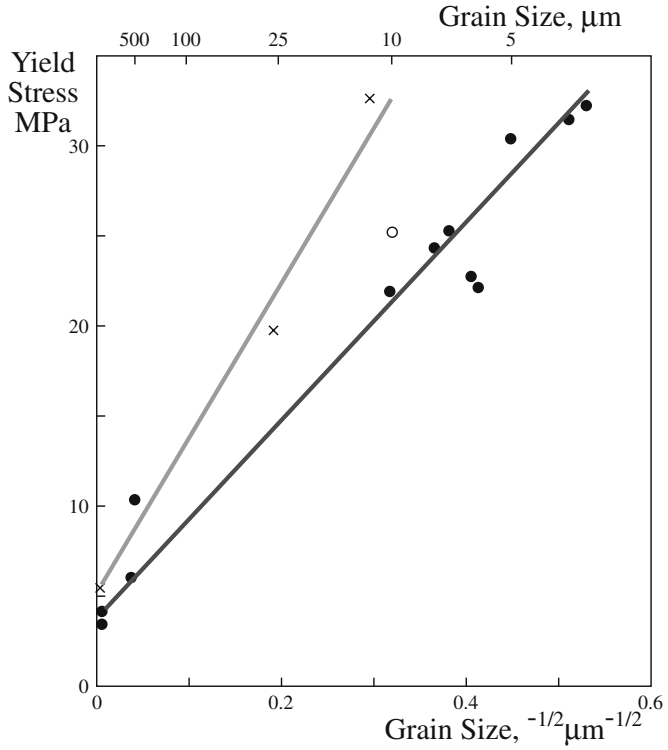

FIGURE 17.10 Grain size dependence of yield strength for KCl. The solid circles are for pure material with a <100> texture; the open circles are for pure material with a <111> texture. The crosses are for Sr-doped KCl.

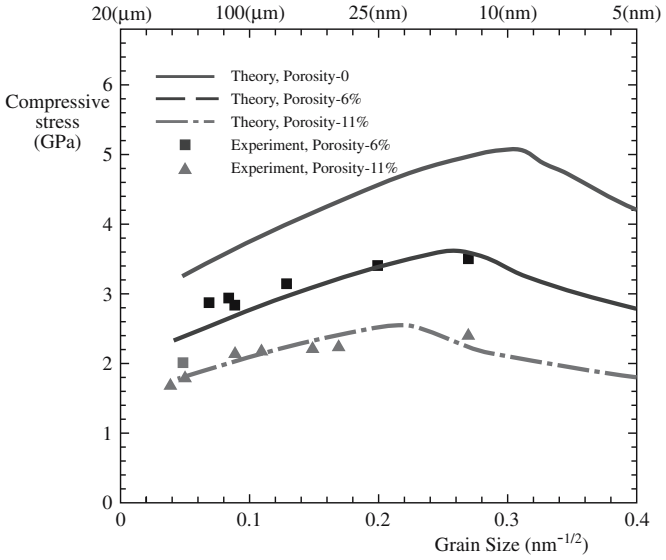

FIGURE 17.11 Compressive yield stress as a function of grain size for nanocrystalline TiO_2 at three levels of porosity.

So the grain size of a polycrystalline ceramic is important in determining the yield strength and the fracture strength of ceramics. Figure 17.9 illustrates the background to Eq. 14.8. Slip starts in the most favorably oriented grains. If the material is to plastically deform then slip must propagate from one grain to the next. Stress concentrations are built up at the grain boundary at P and these are greater when the length of the slip band, or the grain size, is large. For deformation to continue the stress must be sufficient to start dislocation motion in an adjacent grain, which will be easier for large grained samples. The increase in strength of polycrystalline KCl as the grain size decreases (an illustration of the Hall–Petch phenomenon) is shown in Figure 17.10.

In some cases the Hall–Petch equation appears to hold when the grain size is on the order of several nanometers. In these cases deformation cannot be due to dislocation glide and perhaps Eq. 14.8 is best thought of as a scaling law. Figure 17.11 shows a Hall–Petch plot for TiO_2 over a wide range of grain sizes. At the very smallest grain sizes studied the behavior is inverse or negative Hall–Petch. The reasons for this transition are not well understood and the transition does not appear to occur for all nanomaterials.

17.6 DISLOCATION VELOCITY AND PINNING

Figure 17.12 shows the stress dependence of dislocation velocity for CaF_2. At low stresses the relationship has the form

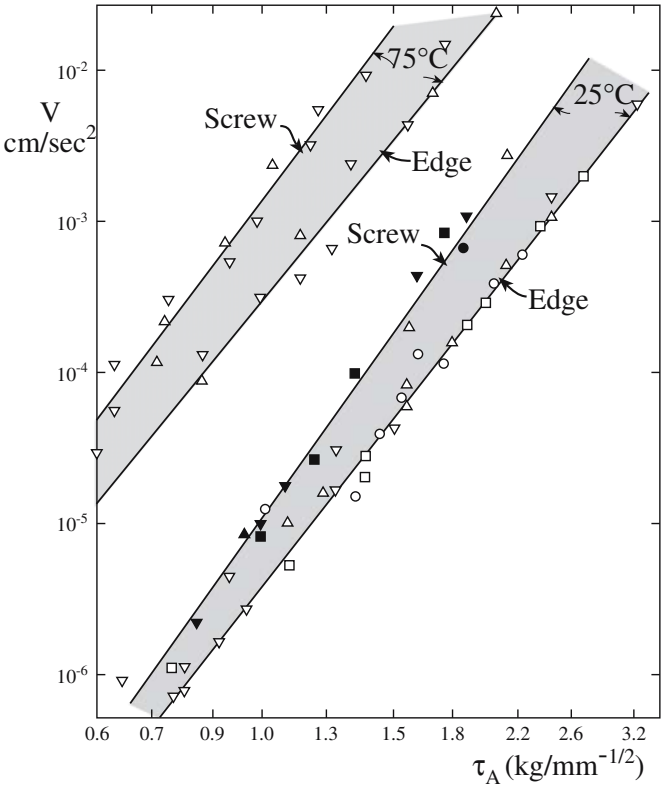

FIGURE 17.12 The stress dependence of dislocation velocity.

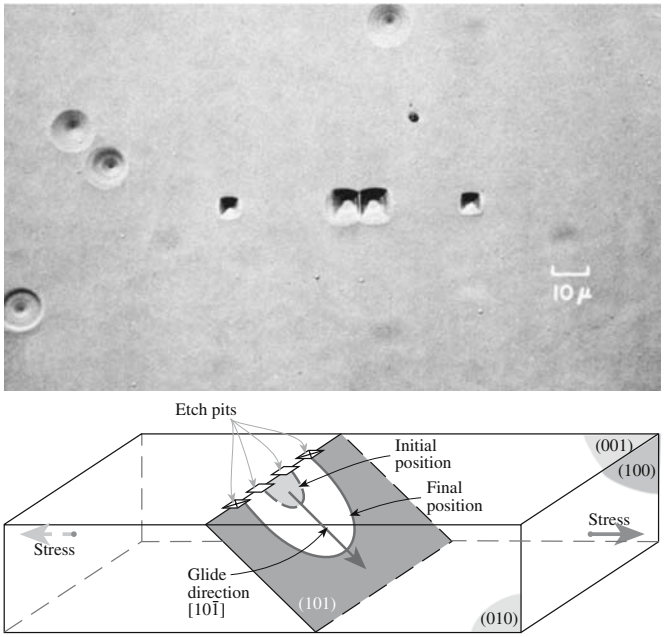

FIGURE 17.13 Etch pits showing the motion of a dislocation loop in single-crystal LiF.

$$v = \left(\frac{\tau}{\tau_0}\right)^p \tag{17.4}$$

Both τ_o and p are material constants: τ_o is the shear stress for unit dislocation velocity and p is the velocity stress exponent that describes the stress dependence of the dislocation velocity. Values are given for some materials in Table 17.5. At very high stresses Eq. 17.4 does not hold, as the maximum dislocation velocity in a crystal equals the velocity of sound. Determination of dislocation velocity has been done using the etch-pit technique as illustrated in Figure 17.13 for LiF.

Dislocations in ceramics can be pinned by solute atoms just as they can in metals as shown in Figure 17.14. The dislocations are impeded because of their interaction with the stress field around the impurity. This effect has long been used to strengthen metals.

TABLE 17.5 Values of the Constants in Eq. 17.4 for Some Materials (RT Except for Ge)

Material	τ_o *(MPa)*	p
Zn	0.03	1
Cu	0.03	1
Mo	64.8	7
Nb	48.3	16
Fe+3%Si	193.1	30
NaCl	1.45	8
LiF	11.7	25
Ge (440°C)	965 GPa	1

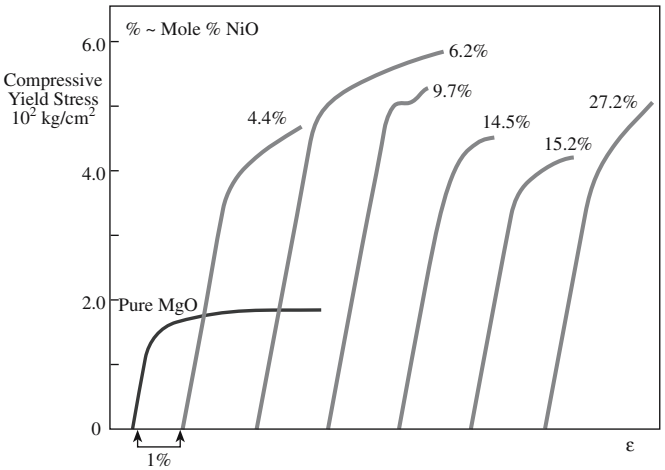

FIGURE 17.14 Illustration of solute hardening in MgO.

17.7 CREEP

Creep is time-dependent permanent deformation that is often due to diffusion processes rather than dislocation motion. Engineers need to consider creep in cases in which ceramic components will be used in load-bearing applications at high temperature. It is necessary to specify a particular maximum strain that is acceptable during the anticipated lifetime of the component.

In general, creep behavior of ceramics is similar to that of metals. However, in ceramics it usually occurs at higher temperatures, typically $>0.5\,T_m$. In comparison, creep is a consideration in aluminum alloys at 100°C and in polymers at room temperature. Creep is particularly important in ice, which creeps extensively at low temperatures. The creep of ice is responsible for the movement of glaciers and the spreading of the Antarctic ice cap.

Figure 17.15 shows a general creep curve. There are three regimes:

- Transient or primary creep: Following a spontaneous elastic strain the creep rate (also referred to as the creep strain rate) decreases with time from an initially high value. This stage of creep is often represented by an equation of the form

$$\varepsilon = \beta T^m \tag{17.5}$$

β is a constant and m varies from 0.03 to 1.0 depending on the material, stress, and temperature. In some ceramics (e.g., SiC fibers) this may be the only stage shown.

- Steady-state or secondary creep: Strain increases linearly with time, the creep rate is constant, and deformation may continue for a long time. This is the most important regime. The equation for secondary creep is

$$\varepsilon = Kt \tag{17.6}$$

K is a constant that depends on stress and temperature. The mechanisms for this stage are discussed in the next sections.

- Tertiary creep: a rapid increase in creep rate just before failure. This stage is often missing for ceramics.

The creep behavior of a ceramic is determined by measuring the stain rate as a function of load. In the simplest approach a load is attached to the sample, which is heated, and the deformation is measured as a function of time. Because of the problems we mentioned earlier in performing tensile tests on ceramics the load is usually applied by bending. The disadvantage of bending tests is the inhomogeneous stress state that changes during creep deformation. The creep behavior of ceramics is different if the load is applied in tension or compression and compressive creep tests may, although rarely, be performed.

There are three mechanisms for creep and we will describe each of these in the following sections.

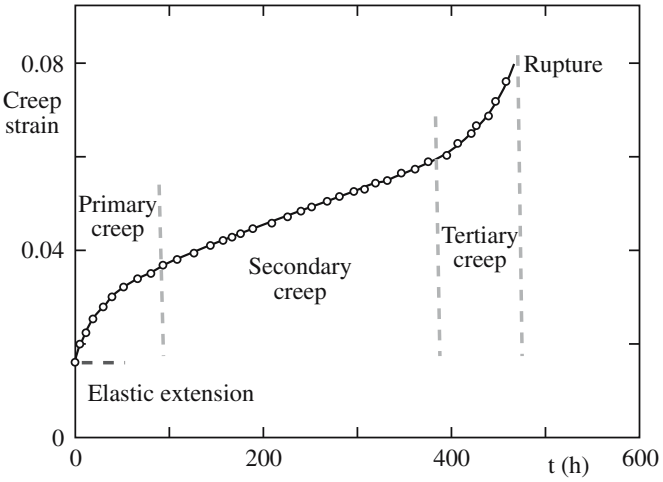

FIGURE 17.15 Creep curve illustrating three distinct regimes.

STRAIN AND CREEP

Elastic strain: $\varepsilon_0 = \sigma/\mathcal{E}$ Creep rate: $\dot{\varepsilon}_c = d\varepsilon_c/dt$ ε_c is the creep strain.

17.8 DISLOCATION CREEP

In this mechanism creep occurs by dislocation motion, i.e., glide and climb. For the climb-controlled process the creep rate can be expressed as

$$\dot{\varepsilon} = \frac{\alpha D_L \mu b}{kT}\left(\frac{\sigma}{\mu}\right)^n \tag{17.7}$$

which we can simplify by taking all of the "constants" into a temperature-dependant constant Γ:

$$\dot{\varepsilon} = \Gamma\sigma^n \tag{17.8}$$

This is a simple power law equation and when $n > 1$ we refer to it as power law creep. For climb n is in the range 4–5; for a glide-controlled process $n = 3$.

17.9 DIFFUSION-CONTROLLED CREEP

TERMS IN CREEP EQUATIONS

α	a constant
D_L	lattice diffusivity
k	Boltzmann's constant
b	Burgers vector
T	absolute temperature
σ	applied stress
μ	shear modulus
m	grain size exponent
n	stress exponent
φ	atomic volume
d	grain size
D_{gb}	grain boundary diffusivity
δ	grain boundary width
A	dimensionless constant
D	diffusion coefficient

In this mechanism creep is due to atomic diffusion. There is no dislocation motion. If we consider the single crystal shown in Figure 17.16 Nabarro (1948) showed that vacancies would move from the faces under tension to those under compression. There will be a counterflow of atoms and we obtain a permanent shape change as a result.

For Nabarro–Herring creep the creep rate is given by

$$\dot{\varepsilon} = \frac{\alpha D_L \sigma \Omega}{d^2 kT} \tag{17.9}$$

In this case the constant, α, depends on the extent of grain-boundary sliding as determined by Herring (1950). For simple tension test measurements under steady-state conditions $\alpha = 13.3$.

We assume the following:

- The main source and sink for vacancies are grain boundaries.
- We are in equilibrium.
- There is no cavitation.

The following important points apply to Nabarro–Herring creep:

- The temperature has to be high enough to allow significant vacancy diffusion.
- Diffusion is considered to occur through the bulk of the material.

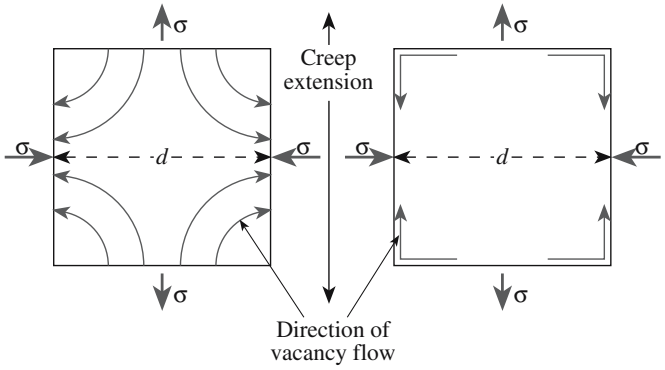

FIGURE 17.16 Illustration of Nabarro–Herring creep.

- Because of the d^{-2} dependence the creep rate will increase with decreasing grain size (shorter diffusion distance).
- The creep rate is proportional to the applied stress (at least for lower stresses).
- There is a linear dependence between strain rate and stress.

At lower temperatures and for fine-grained ceramics grain boundary diffusion may be the dominant path. In these situations the process is termed Coble creep (Coble, 1963) and the creep rate is

$$\dot{\varepsilon} = \frac{150 \Omega \delta D_{gb} \sigma}{\pi d^3 kT} \tag{17.10}$$

The important points to note from Eq. 17.10 are that

- Creep rate varies as d^{-3}; hence it is important for very fine-grained ceramics.
- $D_{gb} > D_L$, so Coble creep is favored at lower temperatures.

Nabarro–Herring and Coble creep can take place in parallel so that actual creep rates will involve both components and both diffusion coefficients. In ceramics we also have a situation in which both anions and cations are diffusing adding further complications to the creep rate equations. If there is a large difference in the diffusion rates then the creep rate is controlled by the slower diffusing species along the faster diffusing path.

17.10 GRAIN-BOUNDARY SLIDING

Some ceramics have an intergranular film (IGF) formed during fabrication, often due to the addition of a sintering aid. If this phase softens at high temperature then we get creep by grain-boundary sliding. The glass viscosity, η, which is a function of temperature, controls the creep rate. As the temperature increases the viscosity decreases, and this is usually represented by an empirical relation known as the Vogel–Fulcher–Tammann (VFT) equation or sometimes simply the Fulcher equation:

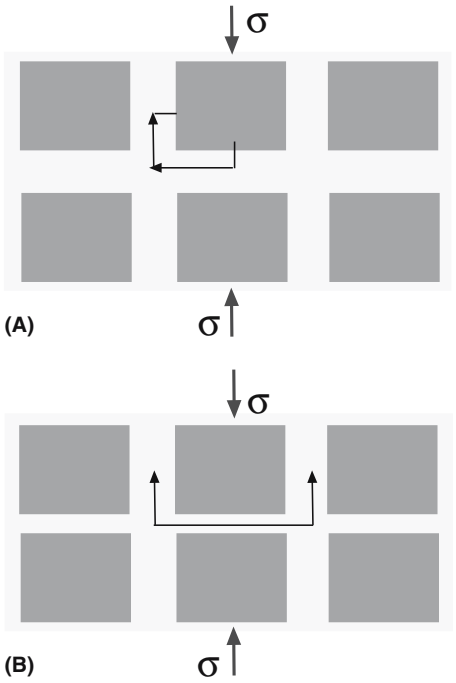

FIGURE 17.17 Illustration of the dissolution–precipitation mechanism that could be operative in ceramics containing a glassy phase at the GB.

$$\ln \eta = A + \frac{B}{T - T_0} \tag{17.11}$$

A, B, and T_0 are constants for a particular glass. The VFT equation works very well except at temperatures close to the glass transition temperature, T_g.

There are several mechanisms that can result in a permanent change in shape. In one mechanism the glass is squeezed out of the boundaries during compression flowing to those under tension. Proof of this mechanism comes from high-resolution TEM, which can be used to directly measure the thickness, w, of the IGF. In these cases

$$\dot{\varepsilon} = \frac{\alpha \omega^3 \sigma}{\eta_0 d^3} \tag{17.12}$$

Another proposed mechanism is that of dissolution and reprecipitation, which is illustrated in Figure 17.17. Here grains dissolve in the liquid at points of high stress, and this solute then diffuses through the liquid and precipitates at regions of low stress. In this case the creep rate is

$$\dot{\varepsilon} = \frac{\alpha \omega \sigma \Omega^{\frac{2}{3}}}{\eta_0 d^3} \tag{17.13}$$

VISCOUS FLOW

Newton's law:

$$\tau = \eta d\gamma/dt$$

This latter mechanism is similar to what happens during liquid-phase sintering (see Chapter 24). The requirements include the following:

- Thep solid must have a certain amount of solubility in the liquid.
- The liquid must wet the solid.

The composition of the IGF is important in determining overall creep behavior. For example, using Y_2O_3 as a sintering aid for silicon nitride ceramics has been found to be superior to using MgO. Other important aspects of the microstructure are the grain size and the volume fraction of liquid present.

17.11 TERTIARY CREEP AND CAVITATION

Tertiary creep represents the final stage of creep deformation and involves an acceleration of the creep rate followed by failure of the component. This stage does not occur in all ceramics, and as previously noted certain ceramics exhibit only primary creep. Tertiary creep involves the formation of cavities that lead to crack formation, often along grain boundaries. The cracks can propagate rapidly, particularly under tensile loading.

Although the nucleation of cavities does not seem to be well understood at present it is clear that cavitation depends on microstructure. Porosity and second-phase particles, which are sources of stress concentration (see Chapter 18), can act as nucleation sites for cavitation and subsequent crack growth. Remember pores can be found in most ceramics; even "pore-free" materials such as hot-pressed alumina may contain small pores. Cavitation also occurs in ceramics with IGFs. Nucleation of the cavities will usually occur at regions where the IGF is not homogeneous, e.g., nonwetted regions, gas bubbles, and impurity particles.

Figure 17.18 shows cavity size distribution data for two polycrystalline aluminas. One is Lucalox (there is no glassy phase) and the other is 99% pure alumina with a glassy phase. The data were obtained using small-angle neutron scattering. For Lucalox the number of pores increases with increasing creep strain but their size does not increase—nucleation is the dominant process. For the alumina with a glassy phase both the number and size of the pores increase with creep strain—we are getting both nucleation and growth.

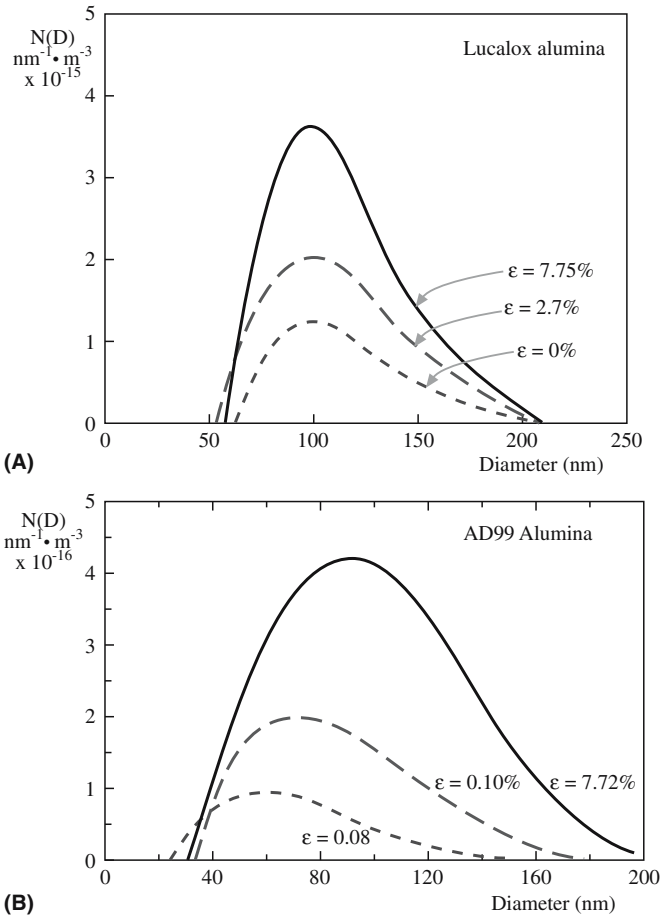

FIGURE 17.18 (a) Cavity-size distribution as a function of creep strain in alumina without a glassy phase (Lucalox). (b) Cavity-size distribution as a function of creep strain in alumina with a glassy phase (AD99).

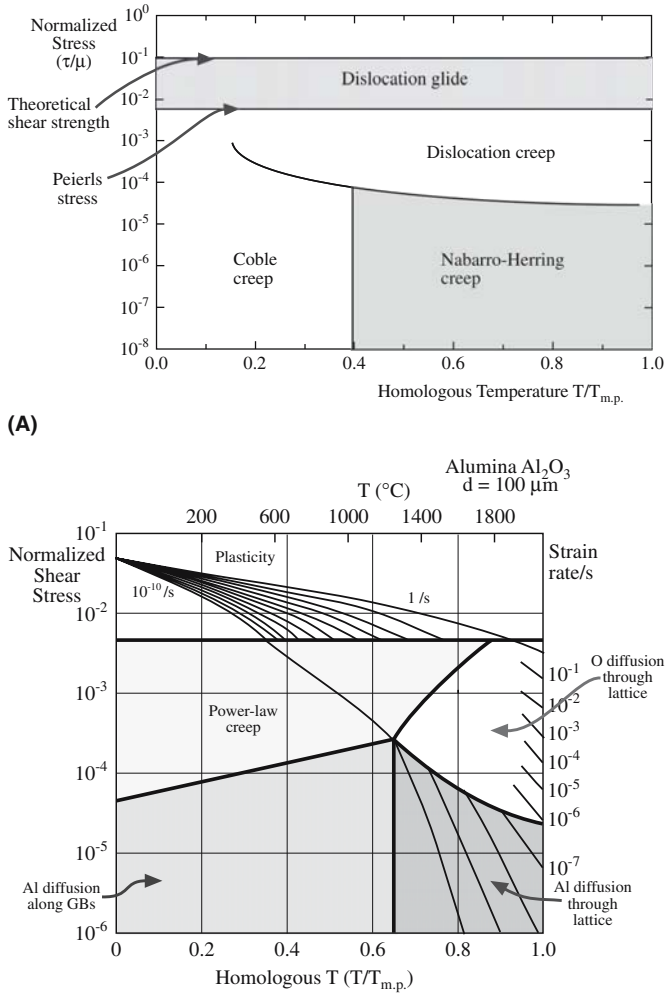

FIGURE 17.19 (a) Schematic of creep deformation map for a polycrystalline ceramic. (b) Creep deformation map for Al_2O_3.

TABLE 17.6 Creep Equation Exponents and Diffusion Paths for Various Creep Mechanisms

Creep mechanism	m	n	*Diffusion path*
Dislocation creep mechanism			
Dislocation glide climb, climb controlled	0	4–5	Lattice
Dislocation glide climb, glide controlled	0	3	Lattice
Dissolution of dislocation loops	0	4	Lattice
Dislocation climb without glide	0	3	Lattice
Dislocation climb by pipe diffusion	0	5	Dislocation core
Diffusional creep mechanisms			
Vacancy flow through grains	2	1	Lattice
Vacancy flow along grain boundaries	3	1	Grain boundary
Interface reaction control	1	2	Lattice/grain boundary
Grain boundary sliding mechanisms			
Sliding with liquid	3	1	Liquid
Sliding without liquid (diffusion control)	2–3	1	Lattice/grain boundary

FIGURE 17.20 Detail from a glass sculpture by Dale Chihuly.

17.12 CREEP DEFORMATION MAPS

From the previous sections you can see that there are a large number of creep mechanisms. These can be expressed by one general equation:

$$\dot{\varepsilon} = \frac{AD\mu b}{kT}\left(\frac{b}{d}\right)^m \left(\frac{\sigma}{\mu}\right)^n \qquad (17.14)$$

The various creep mechanisms give rise to different values of the exponents, m and n, as shown in Table 17.6. For a given ceramic a specific creep mechanism may dominate at certain temperatures and stresses. This can be represented on a creep deformation map as illustrated in Figure 17.19a for a general case and in Figure 17.19b for the specific case of Al_2O_3. These maps are based on a large amount of experimental data.

17.13 VISCOUS FLOW

Viscous flow is an important mechanism for permanent deformation in glasses. It allows us to form complex shapes such as shown in Figure 17.20. Viscous flow is also a mechanism by which ceramics containing IGFs undergo creep. So it is a characteristic that is both beneficial and deleterious, but unavoidable at high temperature.

Under most conditions oxide glasses behave as Newtonian fluids, i.e., the strain rate, $d\gamma/dt$, is a linear function of the applied shear stress, τ. An important consequence of this behavior is that when we draw glasses, such as during the formation of optical fibers, the cross section reduces at a constant rate. In other words, we do not get necking of narrow sections of the fiber. At high stress levels non-Newtonian behavior, which is common in polymers, may be observed in oxide glasses.

Models of viscous flow include the following:

Absolute-rate theory: Viscous flow is a thermally activated process involving a high-energy activated state. Viscosity follows an Arrhenius expression with activation energy for viscous flow, E_v. The preexponential term has a weaker dependence on temperature than the exponential term. This theory is applicable only over a narrow range of temperatures.

Free-volume theory: Molecular motion involves the availability of vacancies. The vacancy volume is the free volume, V_F, of the liquid, approximately the difference in volume of the liquid, V_L, and crystalline, V_c, forms. V_F is a function of temperature. D is a constant close to unity. The Williams–Landel–Ferry (WLF) equation uses a similar approach in which f_g is the fraction of free volume at T_g, about 0.025, and β_L and β_C are the volumetric thermal expansion coefficients of the liquid and solid, respectively.

Excess-entropy theory: There is a decrease in the configurational entropy, S_c, of a liquid when it is cooled down—fewer molecular arrangements are possible. This makes deformation more difficult. E_s is proportional to the potential energy barrier for molecular rearrangement.

EQUATIONS FOR VISCOUS FLOW

Arrhenius:

$$\eta = \eta_0 \exp\left(\frac{E_v}{RT}\right)$$

Turnbull and Cohen:

$$\eta = \eta_0 \exp\left(\frac{DV_c}{V_F}\right)$$

Williams–Landel–Ferry (WLF):

$$\eta = \eta_0 \exp\left[\frac{D}{f_g + (\beta_L - \beta_C)(T - T_g)}\right]$$

Adams–Gibbs:

$$\eta = \eta_0 \exp\left[\frac{E_s}{TS}\right]$$

Vogel–Fulcher–Tammann (VFT):

$$\eta = \eta_0 \exp\left[\frac{C}{T - T_0}\right]$$

The Vogel–Fulcher–Tammann (VFT) equation is an empirical expression relating η to T and can be interpreted in terms of the different models. The VLT expression is accurate over a wide range of temperatures and is widely used in many practical applications.

The viscosity of a specific glass depends on temperature as shown in Figure 17.21. Glass blowing is often performed at viscosities of ~10 MPa·s. This is at the top end of the

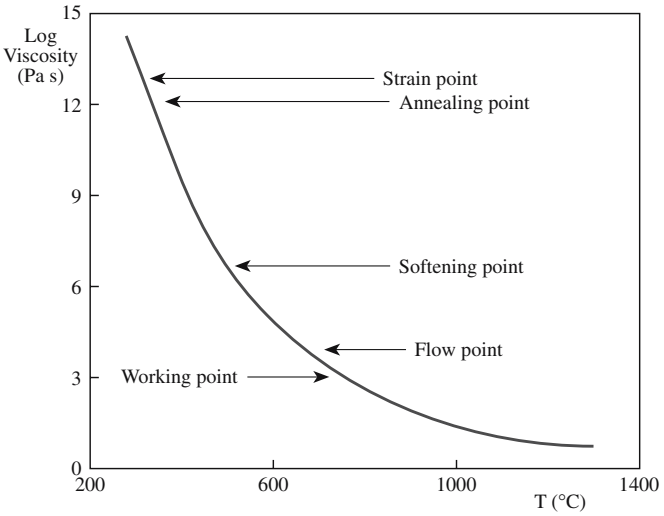

FIGURE 17.21 Temperature dependence of viscosity for a soda-lime-silica glass.

working range, which extends from 1 kPa·s to 10 MPa·s. Figure 17.22 shows a microblown feature formed in a silica scale on oxidized SiC at 1800°C, which for pure silica corresponds to the softening point. If the viscosity was at the fining temperature (~5 Pa·s) the gas would have been able to escape easily. If the viscosity were too high the glass would not have been able to deform in this way.

There is also time dependence to the viscosity, particularly near T_g and above. At these temperatures structural relaxation occurs.

17.14 SUPERPLASTICITY

Superplasticity is the ability of a material to sustain very large strains. From our discussions so far on the mechanical properties of ceramics you may think it unlikely that any ceramic would exhibit superplasticity. But superplasticity has been observed in, for example, tetragonal ZrO_2 stabilized with Y_2O_3. Elongations of 800% were observed for ceramics stabilized with 3 mol% Y_2O_3 and 1038% for tetragonal zirconia stabilized with 2.5 mol% Y_2O_3 containing 5 wt% SiO_2. The general requirements are that the grains should be

- Small (typically < 1 μm)
- Equiaxed

The mechanism for superplasticity in ceramics must clearly be different from that in metal alloys because there

FIGURE 17.22 Microblown silica shape formed on oxidized SiC.

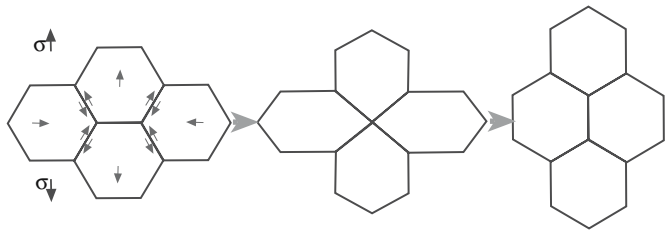

FIGURE 17.23 Model showing how grain switching can produce a shape change.

is no appreciable change in grain shape. Several models have been proposed. The one illustrated in Figure 17.23 involves grain switching and accounts for the constancy of grain shape during deformation, but cannot account for the increase in surface area resulting from plastic deformation. Other models involve grain boundary sliding, but again do not appear to fully account for the process.

Although superplasticity is a useful forming process for metals it tends not to work for ceramics because of the problem of cavitation and the requirement of high temperatures.

CHAPTER SUMMARY

Although we often think of the mechanical properties of ceramics entirely in terms of their brittleness, in this chapter we showed that plastic deformation is also important. The main difference between plasticity in ceramics and in metals is that for ceramics the primary mechanism

of plastic deformation may not be the motion of dislocations. If dislocations are involved then we are invariably at high temperatures. Plastic deformation is a key engineering design consideration in the use of ceramics in structural applications. Consequently, understanding creep behavior is essential, which means we have to understand point defects (Chapter 11) and in many cases the role of IGFs (Chapter 15). As an illustration of why we devoted an entire chapter to this topic remember the example from the final section; elongations in excess of 1000% have been observed in some ceramics. This is clearly not the conventional wisdom when it comes to ceramics and probably something that you would not have expected prior to reading this chapter. Unfortunately, we have not been able to come up with a clear explanation for this property.

PEOPLE IN HISTORY

Herring, W. Conyers, an exception to our rule, is Emeritus Professor of Applied Physics at Stanford University. He has won many major awards and was elected to the National Academy of Sciences in 1968.

Nabarro, Frank Reginald Nunes (1916–2006) is another exception to our rule. He studied at Oxford and Bristol University. During World War II he worked on the explosive effect of shells and was made a member of the Order of the British Empire (OBE). In 1953 he became head of the physics department at the University of the Witwatersrand in South Africa. He is perhaps best known for Nabarro–Herring creep and the Peierls–Nabarro force.

von Mises, Richard (1883–1953) was born in Lemberg, Austria-Hungary, which is now Lviv, Ukraine. A mathematician and engineer he worked in a number of areas including statistics, probability theory, and mechanics. He died in Boston.

GENERAL REFERENCES

Cannon, W.R. and Langdon, T.G. (1983) "Creep of ceramics: Part 1," *J. Mater. Sci.* **18**, 1–80; (1988) "Creep of ceramics: Part 2," *J. Mater. Sci.* **23**, 1.

Chan, K.S. and Page, R.A. (1993) "Creep damage development in structural ceramics," *J. Am. Ceram. Soc.* **76**, 803. A review of creep behavior.

Cook, R.F. and Pharr, G.M. (1994) "Mechanical properties of ceramics," in *Materials Science and Technology*, Vol. 11, edited by M. Swain, VCH Publishers, Weinheim, p. 339.

Davidge, R.W. (1979) *Mechanical Behaviour of Ceramics*, Cambridge, University Press, New York.

Green, D.J. (1998) *An Introduction to the Mechanical Properties of Ceramics*, Cambridge University Press, Cambridge UK.

Nieh, T.G. and Wadsworth, J. (1990) "Superplastic ceramics," *Annu. Rev. Mater. Sci.* **20**, 117.

Poirier, J.-P. (1985) "Creep of crystals: High-temperature deformation processes," in *Metals, Ceramics and Minerals*, Cambridge University Press, Cambridge, UK.

Sprackling, M.T. (1976) *The Plastic Deformation of Simple Ionic Crystals*, Academic Press, London, UK.

Wachtman, J.B. (1996) *Mechanical Properties of Ceramics*, Wiley-Interscience, New York.

SPECIFIC REFERENCES

Buerger, M.J. (1930) "Translation-gliding in crystals of the NaCl structural type," *Am. Mineral.* **15**, 174 and 226.

Coble, R.L. (1963) "A model for boundary diffusion controlled creep in polycrystalline materials," *J. Appl. Phys.* **34**, 1679.

Gilman, J.J. (1959) "Plastic anisotropy of LiF and other rocksalt-type crystals," *Acta. Metall.* **7**, 608.

Hall, E.O. (1951) "The deformation and aging of mild steel: III. discussion of results," *Proc. Phys. Soc.* **B64**, 747.

Herring, C. (1950) "Diffusional viscosity of a polycrystalline solid," *J. Appl. Phys.* **21**, 437.

Nabarro, F.R.N. (1948) in *Report of a Conference on Strength of Solids*, The Physical Society, London, 75. The conference was held at Bristol University in the UK in 1947.

Petch, N.J. (1953) "The cleavage strength of polycrystals," *J. Iron Steel Inst. (London)* **173**, 25.

Reusch, E. (1867) "Ueber eine besondere Gattung von Durchgängen im Steinsalz und Kalkspath," *Ann. Phys. Chem.* **132**, 443 and 449.

EXERCISES

17.1 An MgO single crystal is loaded in uniaxial compression with the [001] direction parallel to the compression axis. Assuming that dislocation motion occurs on the primary slip system when the applied stress is 30 MPa, what is the inherent lattice resistance to dislocation motion?

17.2 The lattice parameter of MgO is $a = 0.4211$ nm. Calculate the distance between Mg^{2+} and O^{2-} ions prior to slip (Figure 17.5a and c) and at the midpoint position (Figure 17.5b and d) during slip on {100} and {110} planes.

17.3 Figure 17.14 shows the hardening effect of NiO additions to MgO. Based on what you know about these two ceramics would you expect the NiO/MgO system to show a complete range of solid solubility? You must justify how you arrived at your answer.

17.4 Figure 17.22 shows a microblown silica shape formed on SiC. What gas do you think would be formed at the SiO_2/SiC interface and lead to the shape shown? Would the gas be different at different temperatures?

17.5 For each of the ceramics listed in Table 17.1 will a tensile stress applied parallel to the *c* axis give a nonzero resolved shear stress?

17.6 The following dislocation reaction has been proposed for dislocation motion in graphite:

$$a/3\ [2\bar{1}\bar{1}0] = a/3\ [1\bar{1}00] + a/3\ [10\bar{1}0]$$

Is the reaction favorable as written? Justify your answer and state any assumptions that you make.

17.7 The addition of impurity atoms can pin dislocations in single crystals. The addition of small amounts (0.002%) of NdF_3 to CaF_2 can be very effective at increasing the yield stress because of the formation of point defect complexes. Using Kröger–Vink notation show that adding NdF_3 to CaF_2 can result in the formation of a defect complex.

17.8 Creep is a concern for structural ceramics at high temperatures. Discuss possible creep mechanisms for SiC and Si_3N_4.

17.9 A major multinational company hires you as a consultant because of your knowledge of ceramics. You are asked to recommend a ceramic that will have the maximum possible creep resistance at an operating temperature of 1200°C. What material would you select and why? Also consider how you would process it.

17.10 Using the data in Figure 17.21 determine the activation energy for viscous flow in the soda-lime-silica glass. Based on your knowledge of glass structures would you expect the activation energy to be higher or lower for a pure silica glass? Briefly justify your answer.